

CrystEngComm

Accepted Manuscript



This is an *Accepted Manuscript*, which has been through the Royal Society of Chemistry peer review process and has been accepted for publication.

Accepted Manuscripts are published online shortly after acceptance, before technical editing, formatting and proof reading. Using this free service, authors can make their results available to the community, in citable form, before we publish the edited article. We will replace this *Accepted Manuscript* with the edited and formatted *Advance Article* as soon as it is available.

You can find more information about *Accepted Manuscripts* in the [Information for Authors](#).

Please note that technical editing may introduce minor changes to the text and/or graphics, which may alter content. The journal's standard [Terms & Conditions](#) and the [Ethical guidelines](#) still apply. In no event shall the Royal Society of Chemistry be held responsible for any errors or omissions in this *Accepted Manuscript* or any consequences arising from the use of any information it contains.

Formation mechanism and elimination methods for anti-site defects in $\text{LiNbO}_3/\text{LiTaO}_3$ crystals

Xueliang Kang^a, Longyue Liang^a, Wei Song^b, Fulei Wang^a, Yuanhua Sang^{*a}, Hong
Liu^{*a}

^a State Key Laboratory of Crystal Materials, Shandong University, 27 Shandan Road, Jinan, 250100, China

^b CETC Deqing Huaying Electronics Co., Ltd, 188 Zhiyuan North Road, Wukang Town, Deqing County, Huzhou, 313200, China

Email: sangyh@sdu.edu.cn (Y. Sang); hongliu@sdu.edu.cn (H. Liu)

Keywords: Lithium niobate, Lithium tantalate, anti-site defect, elimination.

Abstract

Lithium niobate (LiNbO_3 or LN) and lithium tantalate (LiTaO_3 or LT) crystals, which have been widely applied in many fields such as electro-optics, birefringence, nonlinear optics, photorefractive, piezoelectricity and other areas, are reviewed. The studies of the properties and growth techniques are reviewed to give a brief idea for the growth of LN and LT crystals with high quality. The anti-site defects of these crystal materials have been accepted as one of the key factors constraining the improvement of their properties. This review shows simulated calculation and structure of anti-site defects in LN/LT crystals and their effect on the physical properties and summarizes the recent progress in theory and technical processes, including the improved applications. We revised two main methods for elimination of anti-site defect: doping of metal ions and growth of stoichiometric crystals. Finally, the prospects for future studies are outlined.

1. Introduction

Lithium niobate (LiNbO_3 or LN) and lithium tantalate (LiTaO_3 or LT) crystals have been widely applied in many fields, based on their excellent properties in electro-optics, birefringence, nonlinear optics, photorefractive, piezoelectricity and other areas. During recent decades, the crystalline structure, growth, properties, theoretical simulation¹ and applications have been intensively investigated, and substantial progress related to $\text{LiNbO}_3/\text{LiTaO}_3$ materials has been reported.² As is well known, $\text{LiNbO}_3/\text{LiTaO}_3$ crystals are usually grown by a Czochralski (CZ) technique. Due to the crystalline properties of the $\text{Li}_2\text{O-Nb}_2\text{O}_5$ and $\text{Li}_2\text{O-Ta}_2\text{O}_5$ melts, congruent melts are reported to be between 48.38 mol% and 48.6 mol% of Li_2O .³ Therefore, $\text{LiNbO}_3/\text{LiTaO}_3$ crystals grown by the conventional CZ method are non-stoichiometric materials, defined as congruent LiNbO_3 (CLN) and congruent LiTaO_3 (CLT), respectively. Thus, the as-obtained single crystals possess intrinsic defects due to the lack of Li in the lattices. In previous studies⁴, it was proposed that the relatively excess Nb would partially occupy Li vacancies, termed “anti-site Nb (Nb_{Li})”. The influence of anti-site defects on the physical properties of CLN/CLT crystals becomes more and more obvious with the increasing requirements of new applications.⁵ For example, the existence of anti-site defects would significantly decrease the resistance threshold of LN/LT crystals, restricting their laser applications. The existence of anti-site defects would influence the re-alignment of the domain structures,⁶ preventing the fabrication of periodically poled LN/LT wafers. Therefore, the formation mechanism, influences on physical properties and elimination of anti-site defects are the most significant research topics related to the study of the growth and properties of LN/LT crystals. For decades, the formation mechanism has been discussed focusing on the non-stoichiometry of the crystal. Therefore, one basic principle for adjusting the stoichiometry to eliminate the anti-site defects has been

well accepted: eliminating the Li-vacancy with more Li ions or doped ions. Substantial theoretical and technical work has been performed based on this principle. Therefore, it is worthwhile to review the formation and structure of anti-site defects in LN/LT crystals and their effects on physical properties, summarizing the recent advances in both theoretical study and technical processes. Based on the very similar structure and properties of LN and LT crystals, some subjects related to the basic structure and properties have been discussed using the LN crystal as an example. In this review paper, we will give a brief summary of the research history and progress regarding anti-site defects in LN/LT crystals in the following sections: in section 2, we introduce the basic crystal structure and the principle of anti-site defects, and in section 3, we summarize the effect of anti-site defects on the materials' physical properties. In section 4, elimination techniques are summarized, followed by a brief description of the application of LN/LT crystals with a low concentration of anti-site defects. Finally, in section 5, we offer our conclusions and suggestions for future work.

2. Crystal structure and anti-site defects in LN/LT crystals

Because the LN and LT crystals possess similar crystal structure, and the anti-site defects are also similar, we introduce the basic structures in this section with LN as an example. Among all the ferroelectrics, the LN crystal has the highest Curie temperature (approximately 1210 °C) and largest spontaneous polarization (almost 0.70 C/m^2 at ambient temperature)⁷. The LN structure belongs to the trigonal system and can be abstracted as two very different unit cells: hexagonal or rhombohedral. The rhombohedral one is the familiar choice for describing LN structure. As shown in Fig. 1, the structure of LN can be considered as the “stacking” of oxygen octahedrons

along the +c axis with Li and Nb ions filled in them. The octahedrons are coplanar along the +c axis and connected along edges perpendicular to the +c axis. The octahedral interstices are filled by Li ions or Nb ions or are vacant in the following order: ...Nb, V (short for vacancy), Li, Nb, V, Li...⁸. For a convenient description, we introduce the LN structure with a paraelectric phase (Fig. 1(a,b)), which is stable above the Curie temperature. The Nb ions and Li ions are all centered between oxygen layers, achieving charge-balance in the crystal unit. The space group of the paraelectric phase of LN is $R\bar{3}c$. As the temperature decreases from the Curie temperature, for example, the cationic Li and Nb ions in the LN crystal would move along the +c axis. Then, the whole LN crystal exhibits spontaneous polarization, which can only occur along the c axis. This state is familiar as the ferroelectric phase of the LN crystal. The shift of ions also reduces the symmetry of the cell,⁹ and the space group changes to $R3c$ (Fig. 1(c-f)).

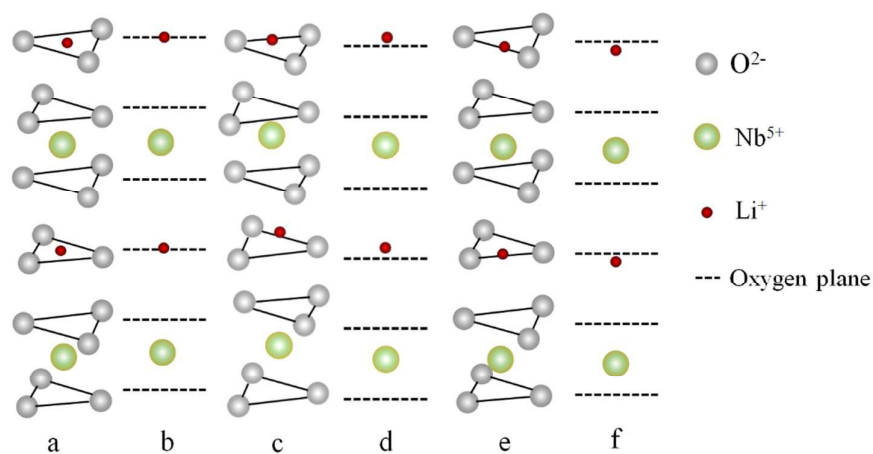


Fig. 1 Structure of LN in paraelectric (a,b) and ferroelectric phases (c-f) with the relative positions of Li ions, Nb ions and oxygen planes.

As is well known, the LN crystal is a typical non-stoichiometric crystal. Its congruent point is disputed and can range from 48.38 mol% to 48.60 mol% of the Li content. The non-stoichiometry of the crystal can be explained based on crystal

chemistry. During crystallization, the Li-O bond in the LN crystal is much weaker than the Nb-O bond,¹⁰ and thus Li vacancies form easily in the unit cell. Therefore, the non-stoichiometric crystal forms due to the lack of Li in the lattice. That is to say, the congruent point of LN crystal is attributed to the intrinsic crystal chemical properties. Therefore, many factors affect the congruent point of LN, including impurities and atmosphere during the crystal growth. Moreover, it is reported that a lack of oxygen in the raw material can influence the congruent point. When the Nb₂O₅ powder lacks oxygen, there should be more Nb in the LN melt than in the normal congruent LN melt. Therefore, during single crystal growth, a crystal with a lower Li/Nb ratio will be crystallized out of the melt, deviating from the congruent point with a lower Li/Nb ratio.¹¹ This phenomenon implies that the congruent point of the LN material might be a macro behavior of the fundamental intrinsic defects. The Li₂O deficiency is crucial for anti-site defect formation. Several structure models have been proposed to describe the anti-site structure, in the effort to advance the theoretical and experimental analysis and seek a strategy to eliminate these intrinsic defects. Among these models, the following three have been widely accepted by materials scientists, solid-state chemists, and condense matter physicists in the research history.

(1) The earliest model of intrinsic defects in LN structure induced by non-stoichiometric composition was the oxygen vacancy model, which was proposed by Fay et al.¹² Its basic viewpoint was that Li vacancies formed due to the lack of Li₂O at the congruent point, while corresponding oxygen vacancies formed for charge compensation. The constitutional formula can be illustrated as [Li_{1-2x}V_{2x}] Nb [O_{3-x}V_x], where the brackets represent the Li and vacancy and the O and vacancy, respectively. This model predicts the crystal density to decrease with greater Li₂O deficiency, which is inconsistent with actual observations.¹³ Therefore, new models have been

proposed to solve the problem.

(2) The second model to explain the non-stoichiometric composition in LN structure is the niobium vacancy model, which was proposed by Peterson et al.¹⁴ This model successfully explains the relationship between the density and Li content of the LN crystal. In this model, no O vacancy is included, and Li vacancies are filled with excess niobium ions. Meantime, some Nb vacancies are generated at the former Nb⁵⁺ sites for charge compensation. The constitutional formula is $[\text{Li}_{1-5x}\text{Nb}_{5x}][\text{Nb}_{1-4x}\text{V}_{4x}]\text{O}_3$. The Nb atoms at Li⁺ sites are usually called “anti-site Nb”, which is the first proposed anti-site defect (Nb_{Li}) in the LN structure. However, Smyth et al.¹⁵ discussed this Nb vacancy model in theory and proposed the unreasonable point. According to this model, in CLN ($[\text{Li}]/[\text{Nb}]=0.942$), there are 5.9 mol% anti-site Nb and 4.7 mol% Nb vacancies. It is believed that such a high charged anti-site Nb concentration in the unit cell is structurally unstable.

(3) The third is the lithium vacancy model, again in which no oxygen vacancies are introduced either. Lerner et al.¹³ proposed that the charge compensation could be achieved by an appropriate amount of Nb ions occupying the corresponding Li vacancies. The proposed formula ($[\text{Li}_{1-5x}\text{V}_{4x}\text{Nb}_x]\text{NbO}_3$) also includes anti-site Nb. There are no Nb vacancies included in this model, which is similar to the lack of Li vacancies in the niobium vacancy model. However, the concentration of anti-site Nb in the Li vacancy model is four times higher than in the Nb vacancy model.

In general, although the Li vacancy model is becoming increasingly popular, the intrinsic defect description model remains debatable. For instance, Peterson and Carnevale¹⁴ analyzed the Nb nuclear magnetic resonance (NMR) and found an additional signal for niobium atoms occupying lithium sites. The intensity of this signal was as high as approximately 6% of the main signal, which could support the

high Nb_{Li} concentration in the Nb vacancy model. Abrahams and Marsh¹⁶ reported that the fine x-ray analysis also indicated a high concentration of Nb_{Li} , which supported the Nb vacancy model. However, the computational simulation of the intrinsic defect structure by Donnerberg et al. indicated that the formation of the niobium vacancy was not favorable¹⁷. Moreover, Safaryan et al.¹⁸ calculated the soft mode frequency and Curie temperature (using ion mass, charge, and the distances between them) to analyze the defect structure of LN crystals with various compositions. The Li vacancy model achieved the simulation values most consistent with the measured values.

In addition, there is also another viewpoint on intrinsic defects in LN crystals. Abdi et al.¹⁹ proposed a new model to describe the intrinsic defects in LN structure, which is based on the coexistence of both Li and Nb vacancies. According to this model, intrinsic defects should include Li vacancies, Nb vacancies and anti-site Nb, and the Nb vacancy and Li vacancy models are simply the two opposite ultimate states of this model. Li et al.²⁰ also supported this type of model by their first-principle analysis within the Slater-Janak transition state model.

In general, the origin of the intrinsic defects in LN/LT crystals is their non-stoichiometric composition. All the models can be attributed to one point, which is the solution of the non-stoichiometric crystal structure with a stable charge equilibrium.²¹ Thus, the strategy to eliminate the intrinsic defects should lean on the realization of stoichiometry, not only by near-stoichiometric LN crystal growth but also by doping to fill the Li vacancy and achieve charge equilibrium.

3. The effect of anti-site defects on the physical properties of LN

As is well known, the physical properties of crystals are influenced and even determined by the crystal defects. As the main class of intrinsic defects of LN crystals,

anti-defects in LN crystals are among the most important factors for the preparation of LN-based devices. Therefore, the effect of anti-site defects on certain physical properties of LN crystals is always a hot research topic, and some great advances have been achieved. Summarizing the research results and the effect of anti-site defects on some important physical properties can not only provide some principle suggestions for crystal growth but also greatly aid in the design and manufacture of LN devices.

1) Dielectric property

The relationship between the electric flux density D and the electric field E is linear, $D = \varepsilon E$, where ε is the second-rank permittivity tensor. As the LN crystal is symmetrical along the c axis, the permittivity is the same for any electric field direction in the plane perpendicular to the c axis. Thus, the permittivity tensor can be represented by the matrix

$$\varepsilon_{ij} = \begin{pmatrix} \varepsilon_{11} & 0 & 0 \\ 0 & \varepsilon_{11} & 0 \\ 0 & 0 & \varepsilon_{33} \end{pmatrix}$$

Permittivity is often normalized in terms of the permittivity of vacuum (ε_0). The dimensionless constant $\varepsilon_{ij}/\varepsilon_0$ is called the relative permittivity or the dielectric constant.²² To measure the dielectric constant, the concepts of ε^T and ε^S will be involved, where ε^T means the crystal is unclamped, such that the stress is zero, and ε^S reflects a clamped crystal in which the strain is zero. The measured values are different and decrease with increasing Li/Nb ratios.²³ As discussed above, the Li/Nb ratio plays a key role in the formation of anti-site defects. As the Li/Nb ratio approaches 1, fewer anti-site defects will be formed in the crystal. The same variation trend is shown in the measured dielectric constants, which indicates that the dielectric property decreases with increasing anti-site defect concentration. Moreover, Abarkan et al.²⁴ have reported that the dielectric coefficients of LiNbO_3 show a relationship

with the doping of Hf. It is reported that Hf ion doping decreases the concentration of anti-site Nb, so the dielectric constant is smaller than for the pure CLN crystal. However, when the Hf doping concentration approaches its threshold, Hf ions will occupy the Nb⁵⁺ site in the lattice, inducing more anti-site Nb,²⁵ and the dielectric constant becomes larger than with lower concentrations of Hf doping.

Xue and Kitamura²⁶ have performed a comprehensive study on the relationship between dielectric properties and anti-site defect concentration in LN single crystals. It is proposed that the anti-site Nb would induce four Li vacancies, which would then induce a certain lattice relaxation. The geometric characteristics of the Nb_{Li} anti-sites or the (Nb_{Li}^{4p})–O bonds are weak compared to Nb ions at the normal Nb⁵⁺ sites, and the geometric characteristics of the Li⁺ site vacancies or the (V_{Li})–O bonds are different from the characteristics of Li ions at the normal Li⁺ sites. Therefore, via the theoretical calculation, the Li⁺ sites in the crystallographic frame of LN are the sensitive lattice sites at which dopants (or vacancies) can modify the dielectric properties most effectively. As the Li/Nb ratio decreases, more anti-site Nb and Li vacancies form, decreasing the dielectric constant of the LN crystal. Therefore, by tuning the stoichiometry of LN, the dielectric property of the LN crystal can be tuned. It also provides a further explanation of how the stoichiometry of the LN crystal influences its dielectric constant. It is believed that the macro state of the stoichiometry of the LN crystal influences the macro dielectric property via the micro-structure defect.

2) Piezoelectric property

The piezoelectric property is an important characteristic of the LN crystal, on which many of its applications are based. In general, the piezoelectric effect refers to the

induced polarization of the crystal under applied stress. The relationship between polarization and stress is linear, and the stress tensor is a second rank tensor, so the piezoelectric tensor should be a third rank tensor, which can be described by a 3×6 matrix. In view of the group symmetry and Neumann's principle, there are only 4 independent coefficients, labeled d_{15} , d_{22} , d_{31} , and d_{33} . Similarly, a piezoelectric crystal also exhibits deformation (strain) under an applied electric field, which is called the converse piezoelectric effect. Its tensor property is the same as the piezoelectric effect.

A few articles have described the relationship between the anti-site defects in LN crystals and the piezoelectric property. Franke et al.²⁷ researched the complex elastic properties of stoichiometric and congruent LN single crystals using an Impedance Analyzer. The results revealed an apparent difference between SLN (stoichiometric LN) and CLN. Finally, they proposed that the difference was caused by defect migration induced by the exo-diffusion of Li ions. In other words, Li ions occupy the Li^+ site in SLN instead of the anti-site Nb ions in CLN, resulting in different piezoelectric properties. Ishizuki et al.²⁸ used MgO-doped CLN crystal as QPM (Quasi-phase matching) device. They found that MgO-doped CLN crystal has a lower coercive field of 4.5 kV/mm than pure CLN crystal at 21 kV/mm. Mg ions will occupy the Li^+ site in the CLN crystal lattice, and such doping ions will help eliminate anti-site defects in LN crystals. Therefore, the anti-site defects would restrict the polarization process by inducing a high conversion voltage.²⁹

3) Optical properties

As a non-linear optical crystal, the optical properties of LN single crystal have been studied widely, including the electro-optic, photovoltaic, photorefractive and refractive index properties.

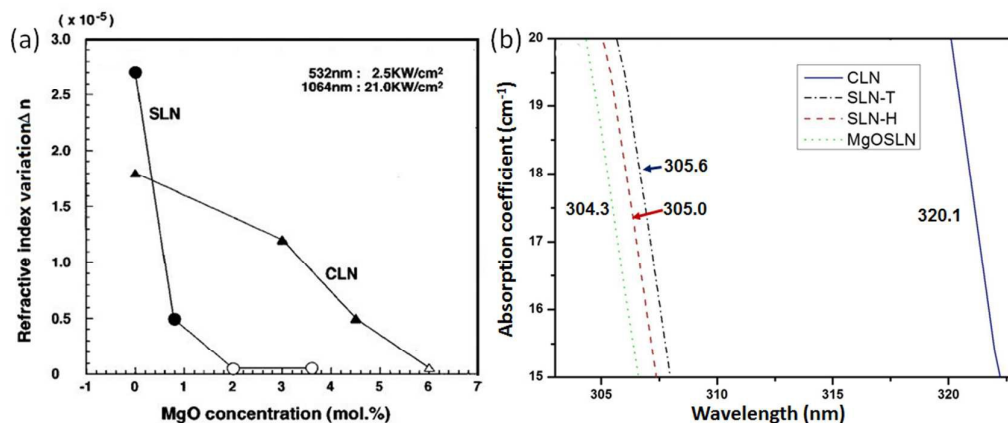


Fig. 2 (a) The refractive index variation in SLN and CLN crystals with various MgO doping concentrations, Reproduced with permission.³¹ Copyright 2001 American Institute of Physics, and (b) the transmittance and absorption of CLN, SLN and MgOSLN. SLN-T and SLN-H stand for the head and tail of a SLN crystal, respectively.

The refractive index is a key coefficient of single crystals, and the LN crystal is a type of uniaxial crystal, whose photorefractive effect is more attractive.³⁰ Furukawa et al.³¹ studied the photorefractive effect of MgO-doped LN using green-induced infrared absorption (GRIIRA). The photorefractive effect in both SLN and CLN crystals decreased monotonically with increasing MgO concentration (Fig. 2(a)). SLN crystals with a high Li/Nb ratio showed a faster decrease of photorefractive effect than congruent crystals. Finally, the photorefractive effect vanishes with MgO doping to the threshold. The significant decrease in GRIIRA over the threshold concentration can be attributed to the complete elimination of intrinsic defects via the incorporation of Mg at Li⁺ sites. Therefore, it can be concluded that the anti-site defects influence the refractive index of LN crystals. In addition, when LN crystals are doped with Bi³⁺, the crystals would introduce new photorefractive centers, hence improving the photorefractive property.³²

Moreover, the adsorption spectra of the LN crystal change with the Li/Nb ratio and MgO doping. Yao et al. compared the transmittance and absorption of CLN, SLN and MgO doped SLN crystals.³³ Fig. 3(b) shows that SLN and MgOSLN crystals have blue-shift absorption edges compared to the CLN crystal. The blue shift can be attributed to the polarizability of O^{2-} in the crystal, and a lower polarizability results in a blue shift of the adsorption edge. The adjacent cation plays an important role in adjusting the polarizability of O^{2-} . Therefore, when the Li concentration in the LN crystal increases, the adjacent cation changes from Nb to Li, resulting in lower O^{2-} polarizability. Thus, the absorption edge shows a blue shift with increasing Li/Nb ratio.³⁴

Xu et al.³⁵ have grown a Pr, Ce co-doped SLN crystal for holography applications. They found that compared to Pr, Ce co-doped CLN crystals, the co-doped SLN crystal has a shorter holographic response time. The diffraction efficiency and the photorefractive sensitivity also show a large improvement. These improved properties are all attributed to the sharp decrease in intrinsic defects in the co-doped SLN crystal.

4) Thermal properties

The thermal properties of the LN crystal mainly include specific heat, thermal expansion, thermal diffusion and thermal conductivity. These thermal properties not only determine the growth habit of the crystal but also help guide the thermal field design during the crystal growth.³⁶

Many scientists have measured the thermal properties of the LN crystal. CLN and SLN crystals have similar specific heat capacities, slightly larger for the SLN crystal. The heat capacities of CLN and SLN crystals, as measured by Zhdanova et al.,³⁷ are $0.648 \text{ J}\cdot\text{g}^{-1}\cdot\text{K}^{-1}$ and $0.651 \text{ J}\cdot\text{g}^{-1}\cdot\text{K}^{-1}$, respectively. The similar specific heat suggests

that specific heat is not greatly influenced by the atomic defects in the crystal.

Thermal expansion obeys a similar rule but is a type of symmetric second-order tensor. Yao et al.³⁸ reported that CLN, SLN and MgOSLN also have similar expansion coefficients along the same direction.

Thermal diffusion is also a second-order tensor. This thermal property is affected by mostly temperature. Not only LN crystals doped with different ions but also the different directions have similar diffusion coefficients, especially in high-temperature regions.

In general, thermal conductivity is the most important thermal property for a single crystal. A higher thermal conductivity is beneficial for the thermal dissipation of LN crystals, which is significant in laser experiments and applications. As shown in Fig. 3, the SLN crystal has the highest thermal conductivity, and the CLN crystal has the lowest. Thermal propagation is the integral effect of phonon transfer. For LN crystals, the anti-site and vacancy defects will significantly influence the phonon transfer by inducing more scattering sites. Therefore, the lower the concentration of atomic defects, the higher thermal conductivity the crystal will possess.

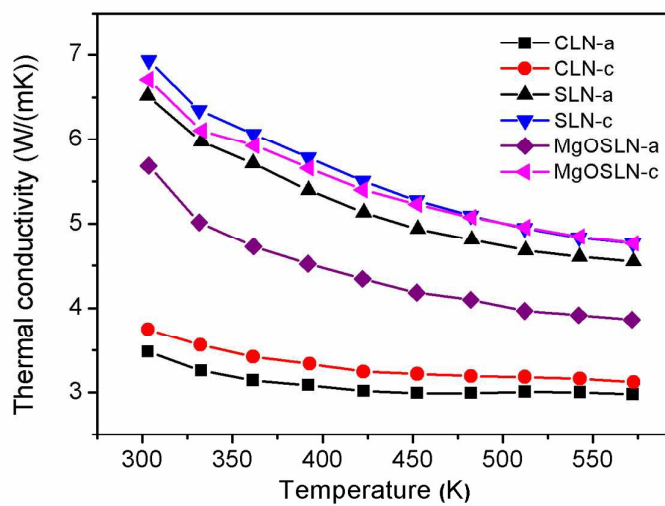


Fig. 3 Thermal conductivity of CLN, SLN and MgOSLN crystals along a- and c-axis.

4. Elimination of anti-site defects and applications

As anti-site defects strongly influence the physical properties of LN/LT crystals, the elimination of anti-site defects is an important issue for the application of these crystals. The main strategies involve doping with metal ions and growing stoichiometric crystals, all based on the reduction of ion vacancies at Li^+ sites.

In general, pure congruent LN/LT crystals are a type of large matrix with anti-site defects, hence with relatively poor physical properties. Upon doping with various metal ions, the crystals form different defect structures, resulting in different properties, and can thus be used in various additional fields.³⁹ Dopant concentration, ionic radii, valence states and others are among the influencing factors. The effects of these factors on the elimination of anti-site defects have been studied. Kling et al.⁴⁰ suggested that dopants with a lower normal valence state than Nb^{5+} ions occupy Li^+ sites; otherwise, they substitute for Nb^{5+} ions. On the other hand, Rebouta et al.⁴¹ paid more attention to the size effect of dopants, or specifically to bond length. They proposed that all dopants with a dopant-O bond longer than the mean length of the Nb-O bond would occupy Li^+ sites. In addition, the doped ions would exhibit a shift from the regular Li^+ sites if the bond is longer than the Li-O bond. Dopants with a bond length less than or equal to the mean length of the Nb-O bond can occupy Li^+ or Nb^{5+} sites. Of course, dopant concentration is also a key factor. It is believed that the dopant would occupy Li^+ or Nb^{5+} sites at a low doping concentration but replace both Li^+ and Nb^{5+} at a high doping concentration. Doping with such a high concentration not only changes the structure of the crystal lattice but also greatly affects the properties. Palatnikov et al.⁴² have observed the anomalous dielectric and piezoelectric properties of heavily doped $\text{LiNbO}_3:\text{Zn}$ crystals, showing that doping

concentration is a key factor in the properties and applications of metal-doped crystals. Luo et al.⁴³ have studied many of the properties of In, Fe, Cu co-doped CLN crystals at various In³⁺ concentrations. In³⁺ ions tend to occupy anti-site Nb and Li vacancies below the threshold concentration. The results of typical two-wave coupling experiments show that the response time shortens, the recording sensitivity improves, and the light-induced scattering decreases with increasing In³⁺ ion concentration, while the diffraction efficiency and the gain coefficient also decrease. Thus, they found an appropriate In³⁺ concentration (2 mol%) to balance these effects.

As discussed by Xue et al.,⁴⁴ the valence of the dopant can induce priority substitution. For instant, a dopant with +2 valence occupies Li⁺ sites, while ions with valence greater than or equal to +5 replace Nb⁵⁺. However, dopants with +3 or +4 valence do not show clear priority substitution. Based on the analysis, the dopant occupancy was proposed to be determined mostly by a parameter d_i , which can be regarded as a pseudopotential that forces the structure to distort:

$$d_i = \left| V_i - \sum_j s_{ij} \right|$$

where V_i stands for the normal valence state of atom i , and s_{ij} stands for the bond valence between atom i and j . Thus, d_i can be interpreted as the degree deviation of the bond valence from the normal state. If the coordination octahedron around the atom i is too large, the average bond length cannot satisfy the bond valence sum rule. Therefore, the sum of the bond valences of the atom i increases as its bond lengths decrease, and vice versa. By calculating the d_i values of various dopant at the Li⁺ and Nb⁵⁺ sites, denoted as d_i^{Li} and d_i^{Nb} , respectively, the dopant would occupy Li⁺ sites if $d_i^{\text{Li}} < d_i^{\text{Nb}}$, otherwise Nb⁵⁺ sites. However, the existence of anti-site Nb should be considered. As $d_i^{\text{Li}} < d_{\text{Nb}}^{\text{Li}} = 1.783$ v.u., the dopant prefers to occupy Li⁺ sites regardless

of the relative values of d_i^{Li} and d_i^{Nb} .

Many works have involved doping LN/LT crystals with various elements to improve the crystal quality.⁴⁵ As reviewed by Kong et al.⁴⁶, among LN:Hf, LN:Zr, LN:Sn; LN:Hf,Fe, LN:Zr,Fe, LN:Zr,Fe,Mn, LN:Zr,Cu,Ce, LN:Ru, LN:V and LN:Mo crystals, LN:Zr,Fe,Mn shows excellent nonvolatile holographic storage properties, and LN:V and LN:Mo have fast response speeds and multi-wavelength storage characteristics. LN:Mo crystals are also used to prepare unusual p-type crystals.⁴⁷ Moreover, the photorefractive properties and photovoltaic effect⁴⁸ can be improved by adjusting the ratio of $\text{Fe}^{2+}/\text{Fe}^{3+}$ in the LN:Fe crystal. In addition, Pracka et al.⁴⁹ reported that the occupation of Cu^{2+} ions in LN crystals depends on the doping process. By a thermal diffusive process, Cu^{2+} takes priority in occupying Li^+ sites, whereas Nb^{5+} sites seem to be occupied by Cu^{2+} ions during the crystal growth. In the research of Dai et al.⁵⁰, doping of Mg^{2+} into Yb^{3+} , Ho^{3+} co-doped LN crystals not only improved optical damage resistance but also increased the optical homogeneity, which improved with increasing Mg^{2+} doping concentration.

While the doping process can eliminate the intrinsic defects, however, it induces other defects called “extrinsic defects”. Different dopants exhibit different defect structures, and studies on each type of dopant have been performed. Here, we take Mg-doped crystal as an example to show a general idea. Mg-doped CLN/CLT crystal is a common material with⁵¹ excellent resistance to optical damage, but its defect structure is still an unsolved question. It is reported that the dopants are able to substitute for anti-site Nb/Ta, Li^+ and $\text{Nb}^{5+}/\text{Ta}^{5+}$ at normal sites. Generally, Mg^{2+} would occupy Li^+ sites. Polgar et al.⁵² suggested that low-concentration doped Mg^{2+} first occupies the Li^+ vacancies and restricts the formation of anti-site Nb. Furthermore, Iyi et al.⁵³ thought that Mg^{2+} would replace two Li^+ ions at normal sites

and form a Li^+ vacancy after substituting all the anti-site Nb. Further doping with Mg^{2+} could result in the substitution of Nb^{5+} at normal sites. However, Liu et al.⁵⁴ noted that occupying the normal Li^+ site and substituting for anti-site Nb occur simultaneously. Mouras et al.⁵⁵ proposed a theory, based on a Raman spectroscopy study, that two Mg concentration ranges can be derived from this investigation. The Mg ions substitute for anti-site Nb and Li vacancies at Mg contents lower than 4 mol% and substitute for both Li and Nb ions at their own sites at Mg contents higher than 4 mol%. The highest doping concentration to eliminate anti-site defects rather than inducing extrinsic defects is called the doping threshold. In practice, 5 mol% MgO doping can achieve the best quality single crystal and is the most acceptable MgO doping threshold for CLN crystals.

Researchers have confirmed the importance of the doping process to improve the crystal quality. However, the traditional solid-state reaction method cannot achieve homogenous doping during crystal growth. A homogenous doping technology is very important for obtaining high-quality single crystals. The wet-chemical method is a useful approach among the various methods for homogeneous ion doping.⁵⁶ In this method, MgO and Li_2CO_3 are all dissolved into citric acid solution, and Nb or Ta can also be dissolved by a series of chemical reactions to form a type of coordination complex. Thus, all the metal ions are dissolved into the liquid phase, achieving a homogeneous mixture. The homogeneous mixing of different ions can be retained via a spray drying process, followed by a heat treatment at 900-1100 °C.⁵⁷ Fig. 4(a,b) show the microstructure of the MgO-doped LN precursor and the calcined polycrystal powder. The precursors are spherical particles approximately 5–10 μm in diameter, transformed into 200-300 nm after calcining. Fig. 4(c,d) show the high quality of the as-grown MgO:CLN crystal. The MgO-doped LN is well grown, and the interference

rings are perfect. In every part of the crystal, the black cross is symmetrical, which indicates that the crystal is of high optical homogeneity.

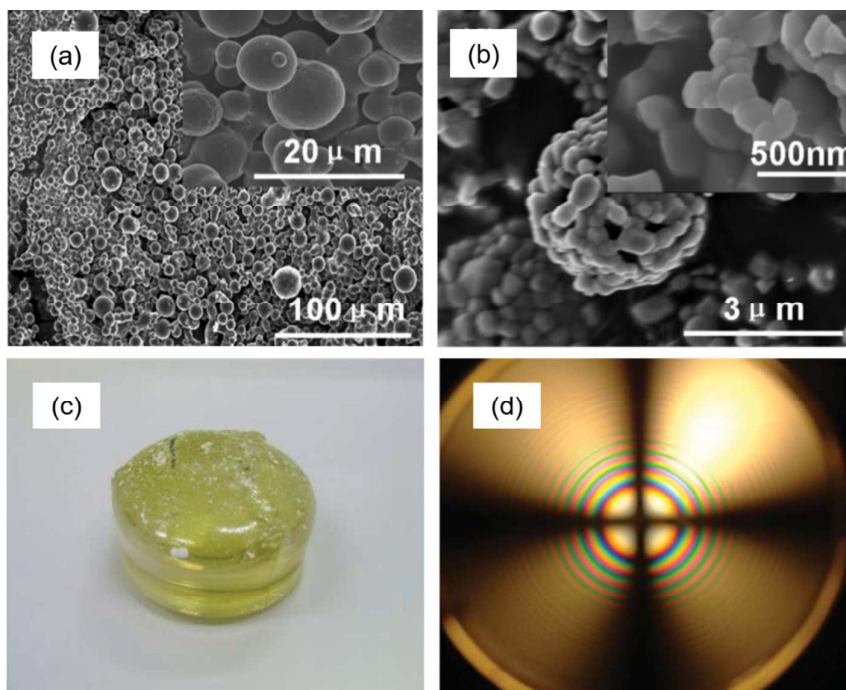


Fig. 4 (a) Scanning electron microscope (SEM) images of the MgO-doped LN precursor and (b) MgO-doped LN powder at 800 °C. Optical image (c) and optical conoscopic interference image (d) of the Mg:LN crystal grown from Mg:LN powder synthesized by the wet chemical-spray drying method. Reproduced with permission.⁵⁶ Copyright 2012, Royal Society of Chemistry.

Moreover, we studied the importance of the homogenous doping of MgO in LT crystals.⁵⁸ MgO-doped CLT/SLT polycrystalline powders were synthesized via the wet route method (labeled as W-Mg:SLT720) and solid-state reaction method (labeled as S-Mg:SLT1200 and S-Mg:CLT1200), respectively, where SLT is stoichiometric LT. The MgO doping by the solid method is not uniform. There are MgO particles retained in the LT polycrystalline powders, as shown by the SEM and the TEM

(transmission electron microscope) images combined with the Mg and Ta element mapping (Fig. 5(a-d)). The anti-site Ta were analyzed via the XPS spectra of three different samples. As shown in Fig. 5(e-g), there is no anti-site Ta in the Mg:SLT sample obtained via the wet-chemical spray-drying method. For the Mg:CLT/SLT samples obtained via the solid-state reaction method, there are two sets of doublets corresponding to Ta^{5+} and Ta^{4+}_{Li} . The anti-site Ta (Ta^{4+}_{Li}) contents for the Mg:SLT and Mg:CLT are 4.9% and 9.8%, respectively. This result indicates that the homogeneous doping of Mg in LT polycrystals can eliminate the formation of anti-site Ta defects, and the proposed wet-chemical spray-drying method can achieve homogeneous doping. Moreover, the anti-site Ta defect concentration of SLT polycrystals is lower than in CLT polycrystals, which is consistent with the effect of stoichiometry on the formation of anti-site defects.

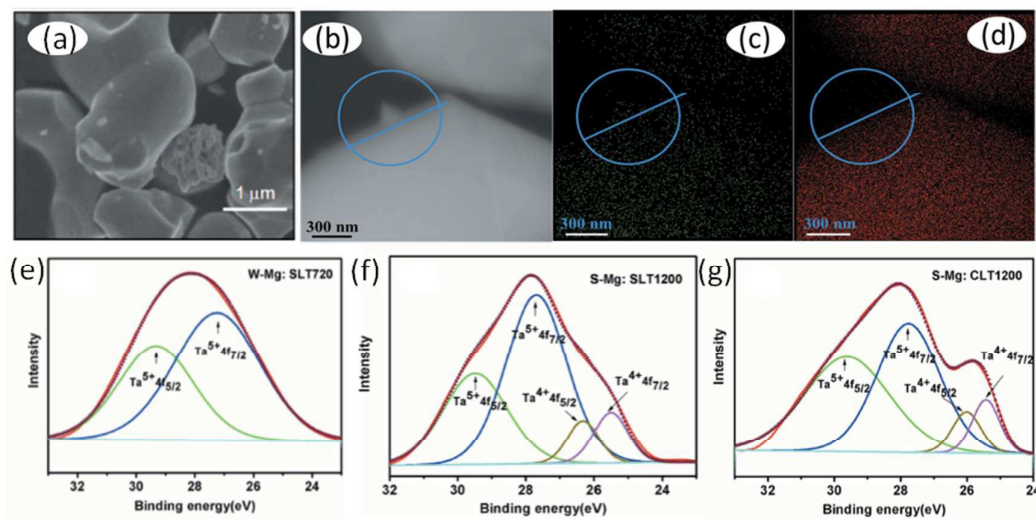


Fig. 5 SEM image of S-Mg:SLT1200 (a), TEM image of S-Mg:SLT1200 (b), Mg element mapping (c) and Ta element mapping (d). The measured Ta_{4f} XPS spectra for the three samples and the decomposition spectra for W-Mg:SLT720 (e), S-Mg:SLT1200 (f) and S-Mg:CLT1200 (g). Reproduced with permission.⁵⁸ Copyright 2015 International Union of Crystallography.

Very recently, by combining the wet-chemical route and the solid-state route, we have proposed a modified method to increase the mass production of homogeneous MgO-doped LN/LT crystalline powders. The principle of this so-called partial-wet process is to mix the Mg^{2+} with other raw materials by ball-milling, then fix the homogeneous dispersion via a spray-drying process followed by a proper heat treatment. In this method,⁵⁹ the doping ions and one of the raw materials, Li_2CO_3 , are dissolved into the citric acid, which consists only of C, H and O. However, another raw material, Nb_2O_5 , remains in particle form and mixes uniformly with the Li ions and doped metal ions by forming a turbid liquid. This partial wet method provides a new concept for crystal powder synthesis and can realize the mass-production of homogeneously Mg-doped LN/LT polycrystalline powders. Moreover, these methods are all universal and can be used broadly in other element doping processes.

As discussed previously, stoichiometric LN/LT single crystal growth is also an efficient route to avoid the formation of high-concentration intrinsic defects. Fig. 6 shows the general process of crystal growth by the CZ method. Thus, there are two steps that can be involved in realizing stoichiometric LN/LT crystal synthesis. The first is SLN/SLT crystal growth. The stoichiometric LN/LT crystals are always grown in melts with a high Li/Nb ratio (approximately 58.5 : 41.5) because lithium tends to volatilize in the melts. The double-crucible method and hanging crucible method with continuous charging system are proposed to achieve a stable Li/Nb ratio during the SLN/SLT single crystal growth.

The second is modifying the CLN/CLT crystals into SLN/SLT crystals. The vapor transport equilibration (VTE) technique⁶⁰ is the most accepted method. Briefly, the congruent crystal wafer is heated in the presence of a Li_2O -rich mixture of powders at

a temperature near the melting point. As a result, Li ions diffuse into the wafer, and the Li/Nb ratio in the wafer increases. With a long diffusion time, an almost stoichiometric composition can be obtained. The flux method involves growing the crystal using a K_2O flux. In this technique, the melt composition of Li:Nb is approximately 1:1, and K_2O is added at more than 6 weight percent (6 wt%) as a flux.

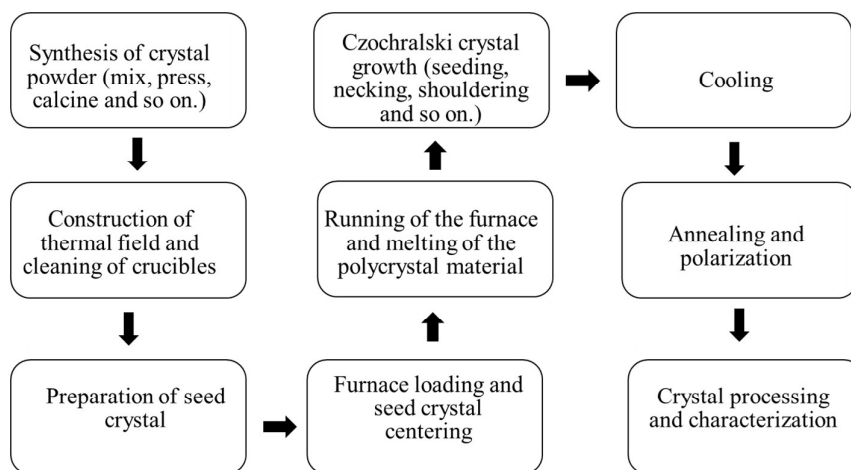


Fig. 6 Schematic diagram of the crystal growth by the CZ method.

SLN crystals and doped CLN or SLN crystals have been widely used because of their excellent properties.⁶¹ The anti-defects in the crystal have been restrained by modifying the Li/Nb ratio or doping with metal ions. The elimination of anti-defects will improve the crystal's physical properties. In addition, the doped metal ions have their own characteristics, which will also modify the whole crystal's properties.

As a nonlinear optical crystal, lithium niobate has been widely applied in the optical field,⁶² such as in the Q-switch, optical parametric oscillator (OPO), and second-harmonic generation (SHG). Examples include the following:

(1) Simple guided optical elements⁶³

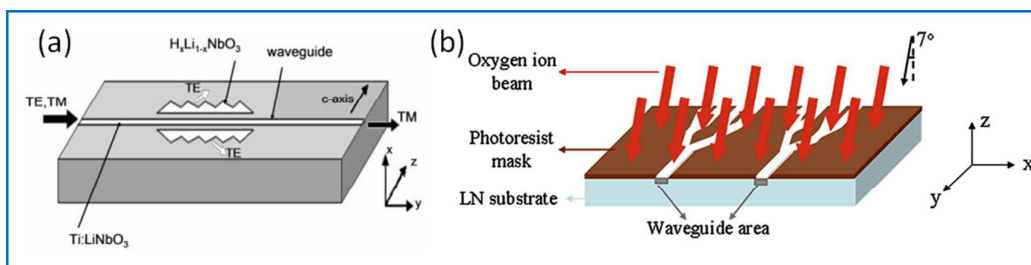


Fig. 7 Integrated waveguide optical polarizer (a). Reproduced with permission.^{63(a)} Copyright 2004 WILEY-VCH Verlag GmbH & Co. KGaA, Weinheim; A schematic of the channel waveguide produced by implanting an O ion in a LN crystal (the implantation region is shown by the gray rectangular area) (b). Reproduced with permission.^{63(b)} Copyright 2010 Elsevier B.V.

As shown in Fig. 7(a), the basic device works by coupling away the TE polarized light propagating in a Ti waveguide by means of coupling to PE (proton exchange) lateral regions, in an X-cut sample with Y propagation. The TM polarization does not couple to those guides and remains localized in the channel Ti waveguide. Moreover, through structure design, other types of optical splitters can be fabricated. The design is of a cascade Y-branch waveguide structure that distributes the input power equally among four output waveguides (Fig. 7(b)).

(2) Nonlinear optical devices

The SHG properties of LN/LT crystals have been widely studied. Here, with a high-quality LN/LT crystal, periodically poled LN/LT (PPLN/PPLT) crystals have been achieved. This type of PPLN or PPLT crystal possesses periodically poled layers and ferroelectric domains arranged alternately on the crystals.⁶⁴ PPLN or PPLT can be used as SHG devices for visible light generation. This type of LN or LT is usually grown by the vapor transport equilibration (VTE) method, which produces different ferroelectric properties from growth by the CZ method. Rostislav et al.⁶⁵ reported the SHG performance of periodically poled vapor transport equilibrated SLN

crystals. A 10 W Nd:YAG laser at 1064 nm was used as a pump, and 1.3 W of green light was generated inside the 1.5 cm long crystal. Similarly, Hum et al.⁶⁶ used a 2 inch SLT crystal grown by the VTE method and generated 10 W of cw (Continuous Wave) 532 nm radiation by SHG with a 2 inch SLT crystal wafer.

Nd- or Yb-doped crystals are mostly of interest for their laser properties. Wang et al. obtained a three-wavelength green laser using the intracavity frequency conversion of Nd:Mg:LiTaO₃ with a MgO:PPLN crystal.⁶⁷ Samples with periods of 7.55 μm (S1), 7.22 μm (S2) and 7.55 & 7.38 & 7.22 μm (S3) were used for the SHG study. Light at 546, 542 and 538 nm was obtained by end pumping with an 808-nm laser diode. The power was 62 mW. The speckle contrast ratio for the three-wavelength laser was only 3.36%, which was only a quarter of the value of the conventional 532-nm laser. PPLN or periodically poled lithium niobate has excellent application prospects. Fig. 8(a) shows a sketch of the laser experimental set, and Fig. 8(b-d) show the laser output spectra of three samples, labeled S1, S2 and S3. With different periods, the samples produced different laser wavelengths.

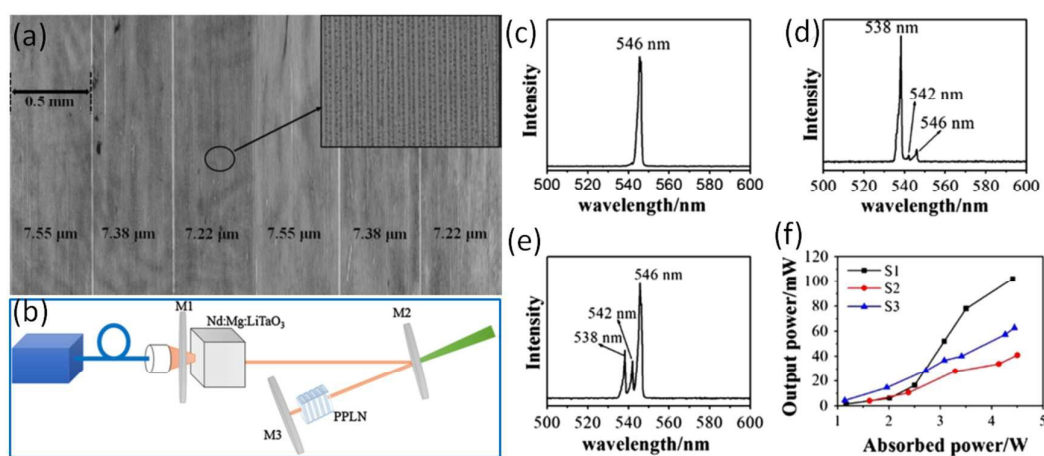


Fig. 8 Periodic structure of S3 (a), experimental setup of the LD-pumped Nd:Mg:LiTaO₃/MgO:PPLN green laser (b), laser spectra for S1 (c), S2 (d), S3 (e), and the output power of the three samples (f). Reproduced with permission.⁶⁷

Copyright Springer-Verlag Berlin Heidelberg 2014.

Moreover, Wang et al.⁶⁸ studied a self-frequency-doubling (SFD) green laser with a Nd:Mg:LiNbO₃ single crystal. The LN crystal is co-doped with Nd and Mg, combining a laser medium and a high-efficiency second harmonic conversion crystal into a single system. The SFD effect was realized via the PPLN crystal with a 7.41 μm poling period fabricated using an electric-field poling process. The laser output power is linear with respect to the pump power (Fig. 9(a)). The maximum green laser output power is 80 mW under 12.4 W of pump power (Fig. 9(b)), which is the best performance reported in the literature.

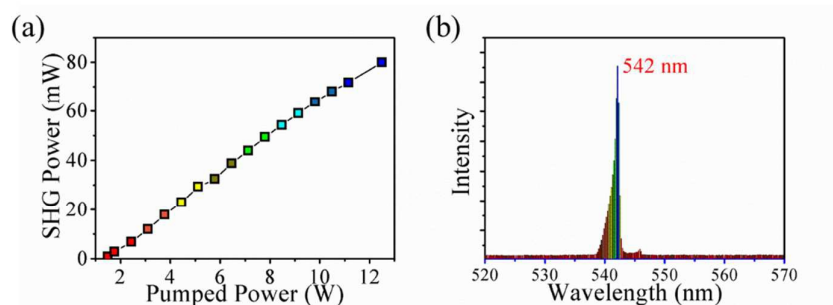


Fig. 9 (a) Output power versus pump power of PPNdMgLN crystal; (b) typical laser spectrum of SFD green laser. Reproduced with permission.⁶⁸ Copyright 2015 Optical Society of America

5. Summary and perspective

There is increasing work related to the formation and elimination of anti-site defects, implying the importance of this topic to the growth of high-quality single LN/LT crystals. The application of these crystals requires high quality with low intrinsic defect concentrations. Therefore, we summarize the recent advances related to the fundamental studies of anti-site defects and methods elimination, along with the recent applications using these crystals at low defect concentrations. Briefly, the

formation of these intrinsic defects in LN/LT crystals is induced by the non-stoichiometric composition during single crystal growth, resulting in a shortage of Li in the lattices. The relatively excess Nb partly occupies Li vacancies, forming anti-site Nb defects. In addition, there should be complex occupation to reduce the concentration of Li vacancies, which has been described by several proposed intrinsic defect models, such as the oxygen vacancy model, the niobium vacancy model, and the lithium vacancy model.

Based on the original formation of anti-site defects, the key point in eliminating these intrinsic defects is reducing the Li vacancy concentration. Elemental doping and stoichiometric crystal growth are the most accepted routes to reduce the Li vacancy concentration. The doped or stoichiometric LN/LT crystals possess improved electro-optic, birefringence, nonlinear optic, photorefractive, and piezoelectricity properties, compared with the crystals grown by conventional technique. Meanwhile, ion doping and stoichiometric crystal growth make the crystal growth more difficult. In this situation, the homogeneity of chemical composition, crystal structure, and physical properties of the doped crystals and SLN or SLT should be paid more attention. For instant, the relationship between local crystal structure or chemical composition and electric domain structure in micro-scale should be clarified, which can provide basic guide for PPLN fabrication. In addition, the influence of applied electric field or light on the crystal structure or size of unit cell should be in situ studied in micro-scale, which is important to understand the behaviour of laser in crystal, and to develop new applications in laser related fields. Moreover, because most of the modern applications of LN/LT crystals require crystals with high quality and large size to match the requirement of microfabrication process, the large-size crystals, especially large-size stoichiometric LN/LT crystals, are urgently demand.

Therefore, more reliable simulation method software and more fine controllable growth technique are required to get rid of problems about the inhomogeneity of the as-grown crystals. A technique for growth of large-size crystal with strict stoichiometry will be highly demanded, which is still a great challenge.

6. Acknowledgements

The authors are thankful for fundings from the National Natural Science Foundation of China (Grant No. 51402172), Innovation Research Group (IRG: 51321091), National High Technology Research and Development Program of China (863 Program, Grant No. 2013AA030501).

Received: ((will be filled in by the editorial staff))

Revised: ((will be filled in by the editorial staff))

Published online: ((will be filled in by the editorial staff))

-
- 1 S. Kato, S. Kurimura and N. Mio, *Opt. Mater. Express*, 2016, **6**, 396-401.
 - 2 T. Yan, Y. G. Yu, Y. J. Guo, Y. H. Sang, H. Liu, S. Q. Sun, M. Xu, J. Y. Wang, L. W. Chang and M. M. C. Chou, *J. Alloys Compd.*, 2013, **564**, 1-7.
 - 3 P. F. Bordui, R. G. Norwood, C. D. Bird et al. *Appl. Phys. Lett.*, 1968, **12**, 92.
 - 4 T. Yan, Y. H. Leng, Y. G. Yu, D. H. Sun, J. Zhan, W. H. A. Kamaruddin, X. Y. Qin, X. X. Shi, L. W. Chang, M. M. C. Chou, J.Y. Wang and H. Liu, *CrystEngComm*, 2014, **16**, 6593.
 - 5 E. Wendler, G. Becker, J. Rensberg, E. Schmidt, S. Wolf and W. Wesch, *Nucl. Instr. Meth. B*, 2016, DOI: 10.1016/j.nimb.2016.03.007.
 - 6 V. I. Pryakhina, D. O. Alikin, S. A. Negashev and V. Y. Shur, *Ferroelectrics*, 2016, **496**, 79-84.
 - 7 Y. F. Kong, J. J. Xu, G. Y. Zhang, S. M. Liu and Y. Lu, *Multifunctional photoelectric material—Lithium Niobate crystals*, Science Press, Beijing, 2005.
 - 8 a) R. J. D. Tilley, *Perovskites: Structure-Property Relationships*, John Wiley & Sons, Ltd, Manhattan, 2016; b) R. S. Weis and T. K. Gaylord, *Appl. Phys. A*, 1985, **37**, 191-203.
 - 9 Y. Noguchi, R. Inoue and M. Miyayama, *Adv. Condens. Matter. Phys.*, 2016, **2016**,

-
- 10.
- 10 a) J. Piecha, A. Molak, U. Breuer, M. Balski and K. Szot, *Solid State Ionics*, 2016, **290**, 31–39; b) S. C. Abrahams, J. M. Reddy and J. L. Bernstein, *J. Chem. Phys. Solids*, 1966, **27**, 997; c) S. C. Abrahams, W. C. Hamilton and J. M. Reddy, *J. Chem. Phys. Solids*, 1966, **27**, 1019.
- 11 a) Y. S. Kuzminov and V. V. Osiko. *Ferroelectrics*, 1993, **142**, 105; b) S. Erdei and F. W. Ainger. *J. Cryst. Growth*, 1997, **174**, 293; c) F. P. Safaryan, R. S. Feigelson and A. M. Petrosyan, *J. Appl. Phys.*, 1999, **85**, 8079.
- 12 H. Fay, W. J. Alford and H. M. Dess. *Appl. Phys. Lett.*, 1968, **12**, 69.
- 13 P. Lerner, C. Legras and J. P. Dumas, *J. Cryst. Growth*, 1968, **3/4**, 231.
- 14 G. E. Peterson and A. Carnevale, *J. Chem. Phys.*, 1972, **56**, 4848.
- 15 D. M. Smyth, *Ferroelectrics*, 1983, **50**, 93.
- 16 S. C. Abrahams and P. Marsh, *Acta Crystallogr.*, 1986, **B42**, 61.
- 17 H. Donnerberg, S. M. Tomlinson, C. R. A. Catlow and O. F. Shirmer, *Phys. Rev. B*, 1989, **40**, 11909.
- 18 F. P. Safaryan, R. S. Feigelson and A. M. Petrosyan, *J. Appl. Phys.*, 1999, **85**, 8079.
- 19 F. Abdi, M. D. Fontana, M. Aillerie and P. Bourson, *Appl. Phys. A*, 2006, **83**, 427–434.
- 20 Y. L. Li, S. Sanna and W. G. Schmidt, *J. Chem. Phys.*, 2014, **140**, 23.
- 21 Y. L. Li, W. G. Schmidt and S. Sanna, *Phys. Rev. B*, 2015, **91**, 174106.
- 22 R. S. Weis and T. K. Gaylord, *Appl. Phys. A*, 1985, **37**, 191–203.
- 23 a) A.W. Warner, M. Onoe, G.A. Coquin, *J. Acoust. Soc. Am.*, 1967, **42**, 1223–1231; b) A. Savage, *J. Appl. Phys.*, 1966, **37**, 3071–3072; c) R.T. Smith and F.S. Welsh, *J. Appl. Phys.*, 1971, **42**, 2219–2230; d) T. Yamada, N. Niizeki and H. Toyoda, *Jpn. J. Appl. Phys.*, 1967, **6**, 151–155; e) J. R. Teague, R. R. Rice and R. Gerson, *J. Appl. Phys.*, 1975, **46**, 2864–2866.
- 24 M. Abarkan, M. Aillerie, J. P. Salvestrini and M. D. Fontana, 2008, arXiv:0808.2802.
- 25 X. N. Shen, W. B. Yan, J. L. Jing, L. H. Shi, F. F. Jia, G. H. Liang, Y. Y. Huang, M. Wu, Y. W. Zhang, H. Y. Dong, J. S. Zhang, G. F. Chen and H. J. Chen, *J. Mater. Sci.*, 2014, **49**, 3775–3779.
- 26 D. Xue and K. Kitamura, *Solid State Commun.*, 2002, **122**, 537–541.
- 27 I. Franke, J. Salvestrini, M. Fontana and Krystian, *Ferroelectrics*, 2004, **304**, 155–158.
- 28 H. Ishizuki, I. Shoji and T. Taira, *Appl. Phys. Lett.*, 2003, **82**, 4062.
- 29 a) X. J. Wang, F. Bo, S. L. Chen, J. Chen, Y. F. Kong, J. J. Xu and G. Q. Zhang, 2015 Conference on Lasers and Electro-Optics, San Jose, CA, May, 2015; b) A. El-Bachiri, F. Bennani and M. Boussemti, *Spectrosc. Lett.*, 2014, **47**, 374–380.
- 30 M. Unferdorben, Z. Szaller, I. Hajdara, J. Hebling and L. Pálfalvi, *J. Infrared, Millimeter, Terahertz Waves*, 2015, **36**, 1203–1209.
- 31 Y. Furukawa, K. Kitamura, A. Alexandrovski, R. K. Route, M. M. Fejer and G. Foulon, *Appl. Phys. Lett.*, 2001, **78**, 14.
- 32 D. H. Zheng, Y. F. Kong, S. G. Liu, M. L. Chen, S. L. Chen, L. Zhang, R. Rupp and J. J. Xu, *Sci. Rep.*, 2016, **6**, 20308.
- 33 S. H. Yao, X. B. Hu, J. Y. Wang, H. Liu, L. Gao, X. F. Cheng, X. Yin and X. F. Chen, *Cryst. Res. Technol.*, 2007, **42**, 114–118.
- 34 a) T. Zhang, B. Wang, F. Ling, S. Fang and Y. Xu, *Chem. Phys.*, 2004, **83**, 350–353; b) X. H. Zhen, L. C. Zhao and Y. H. Xu, *Appl. Phys. B*, 2003, **76**, 655.

-
- 35 Z. P. Xu, X. Zhang, S. D. Zhang, L. J. Jin, J. Q. Tong and J. Gao, *Optik (Munich, Ger.)*, 2015, **126**, 1591–1594.
- 36 Y. Z. Zhu, S. P. Lin, Y. Zheng, D. C. Ma and B. Wang, *J. Mater. Sci.*, 2016, **51**, 3155–3161.
- 37 V. V. Zhdanova, V. P. Klyuev, V. V. Lemanov, I. A. Smirnov and V. V. Tikhonov, *Fiz. Tverd. Tela.*, 1968, **10**, 1725–1728.
- 38 S.H. Yao, J.Y. Wang, H. Liu, T. Yan, D. H. Yu and Y. F. Chen, *J. Cryst. Growth*, 2011, **318**, 951–953.
- 39 X. J. Wang, X. Zhang, L. J. Jin, J. Q. Tong, J. Gao, Z. P. Xu, *Int. Soc. Opt. Photonics*, 2015, **9522**, 95222H.
- 40 A. Kling, C. Valdre, J. G. Marques, M. F. Da Silva and J. C. Soares, *Nucl. Instrum. Methods Phys. Res. B*, 2002, **190**, 524.
- 41 L. Rebouta, P. J. M. Smulders, D. O. Boerma, F. Agullo-Lopez, M. F. Da Silva and J. C. Soares, *Phys. Rev. B*, 1993, **48**, 3600.
- 42 M. N. Palatnikov, V. A. Sandler, N. V. Sidorov and O. V. Makarova, *Inorg. Mater.*, 2016, **52**, 147–152.
- 43 S. H. Luo, Q. X. Meng, J. Wang and X. D. Sun, *Opt. Commun.*, 2016, **358**, 198–201.
- 44 a) D. F. Xue and X. K. He, *Phys. Rev. B*, 2006, **73**, 064113; b) K. Y. Li, C. Kang, and Dongfeng Xue. *Mater. Focus*, 2015, **4**, 28–31.
- 45 N. V. Sidorov, A. A. Yanichev, M. N. Palatnikov and A. A. Gabain, *Opt. Spectrosc.*, 2014, **116**, 281–290.
- 46 Y. F. Kong, S. G. Li and J. J. Xu, *Mater.*, 2012, **5**, 1954–1971.
- 47 T. Tian, Y. F. Kong, H. D. Liu, S. G. Liu, W. Li, S. L. Chen, J. J. Xu, J. Y. Xu and H. B. Zeng, *J. Mater. Sci: Mater. Electron.*, 2016, **27**, 5886–5891.
- 48 a) Y. Noguchi, R. Inoue and M. Miyayama, *Adv. Condens. Matter Phys.*, 2016, **10**, 2943173; b) A. Sanson, A. Zaltron, N. Argiolas, C. Sada, M. Bazzan, W. G. Schmidt and S. Sanna, *Phys. Rev. B*, 2015, **91**, 094109.
- 49 I. Pracka, A. L. Bajor, S. M. Kaczmarek, M. Wirkowicz, B. Kaczmarek, J. Kisielewski and T. Ukasiewicz, *Cryst. Res. Technol.*, 1999, **34**, 627–634.
- 50 L. Dai, S. S. Jiao, Z. H. Yan, P. Dai, G. Lui and Y. H. Xu, *Mod. Phys. Lett. B*, 2016, **30**, 1550260.
- 51 N. A. Chaitanya, M. V. Jabir and G. K. Samanta, 2016, arXiv:1601.02374v1.
- 52 K. Polgar, L. Kovacs, I. Foldvari and I. Cravero, *Solid State Commun.*, 1986, **95**, 375.
- 53 N. Iyi, K. Kitamura, Y. Yajima, S. Kimura, Y. Furukawa and M. Sato, *J. Solid State Chem.*, 1995, **118**, 148.
- 54 J. J. Liu, W. L. Zhang and G. Y. Zhang, *Phys. Stat. Sol.(A)*, 1996, **156**, 285.
- 55 R. Mouras, M. D. Fontana, P. Bourson and A. V. Postnikov, *J. Phys.: Condens. Matter.*, 2000, **12**, 5053–5059.
- 56 Q. B. Liu, D. H. Sun, T. Yan, F. F. Zheng, Y. H. Sang, H. Liu, J. Y. Wang and T. Ohachi, *CrystEngComm*, 2012, **14**, 5572–5578.
- 57 S. H. Yao, F. Zheng, H. Liu, J. Y. Wang, H. J. Zhang and T. Yan, *Cryst. Res. Technol.*, 2009, **44**, 1235–1240.
- 58 D. H. Sun, X. L. Kang, Q. Yu, K. Cui, X. Y. Qin, X. X. Shi, H. Q. Cai, T. Ohachi, Y. H. Sang and H. Liu, *J. Appl. Cryst.*, 2015, **48**, 377–385.
- 59 Y. H. Sang, D. H. Sun, X. L. Kang, L. Y. Liang, D. Z. Wang, Y. Feng, Y. J. Qiao and H. Liu, *PRC Pat.*, 103922405, 2014.
- 60 a) J. Hirohashi, *Characterization of domain switching and optical damage*

-
- properties in ferroelectrics*, Royal Institute of Technology, Stockholm, 2006; b) R. Bhatt, I. Bhaumik, S. Ganesamoorthy, A. K. Karnal, P. K. Gupta, M.K. Swami, H.S. Patel, A.K. Sinha and A. Upadhyay, *J. Mol. Struct.*, 2014, **1075**, 377-383.
- 61 a) Y. L. Li, W. G. Schmidt and S. Sanna, *Phys. Rev. B*, 2015, **91**, 174106; b) S. T. Murphy and N. D. M. Hine, *Chem. Mater.*, 2014, **26**, 1629-1638.
- 62 S. Kato, S. Kurimura and N. Mio, *Opt. Mater. Express*, 2016, **6**, 396-401.
- 63 a) L. Arizmendi, *Phys. Stat. Sol. (a)*, 2004, **201**, 253-283; b) J. Zhao, X. Wang and F. Chen, *Opt. Mater.*, 2010, **32**, 1441.
- 64 N. C. Carville, S. M. Neumayer, M. Manzo, M. Baghban, I. N. Ivanov, K. Gallo and B. J. Rodriguez, *J. Appl. Phys.*, 2016, **119**, 054102.
- 65 R. V. Roussev, R. Route, J. Schaar, K. Urbanek, M. M. Fejer, D. Jundt and C. Kajiyama, *Proc. of SPIE*, 2006, **6103**, 610302.
- 66 D. S. Hum, R. K. Route, G. D. Miller, V. Kondilenko, A. Alexandrovski, J. Huang, K. Urbanek, R. L. Byer and M. M. Fejer, *J. Appl. Phys.*, 2007, **101**, 093108.
- 67 D. Z. Wang, B. X. Yan, Y. Bi, D. H. Sun, Y. H. Sang, H. Liu, A. Kumar and R. I. Boughton, *Appl. Phys. B*, 2014, **117**, 1117-1121.
- 68 D. Z. Wang, D. H. Sun, X. L. Kang, Y. H. Sang, B. X. Yan, H. Liu and Y. Bi, *Opt. Express*, 2015, **23**, 17727-17738.



Kang et al. summarized the mechanism of formation of anti-site defect in $\text{LiNbO}_3/\text{LiTaO}_3$ crystals and the measures for growth of anti-site defect free $\text{LiNbO}_3/\text{LiTaO}_3$ crystals to give the readers an overview in this field.